MAGNETIC RESONANCE IN MEDICINE 8, 275–284 (1988)

Simultaneous Multislice Acquisition of MR Images

JOHN B. WEAVER

Diagnostic Radiology, Dartmouth-Hitchcock Medical Center, Hanover, New Hampshire 03756

Received January 19, 1988; revised May 12, 1988

The simultaneous multislice technique is a method of imaging multiple parallel slices with the number of echoes normally used to image a single slice. Images of 16 slices have been obtained from a single 128-echo acquisition. The distance between the slices can be decreased to approximately 15% of the field of view in the readout direction with the cost of significant image blurring. The image blurring is negligible when the distance between the slices approaches the field of view in the readout direction. The trade-offs are described, and equations and images are presented.

INTRODUCTION

It is important to minimize MRI measurement time both because it is expensive and because it is difficult to image moving anatomy. Multiple-echo and multiple-slice imagings are important for this purpose. Shorter imaging times are one of the major advantages of low-RF-angle, gradient-refocused imaging, e.g., FLASH (*1–3*).

A method of multiplexing several slices into one acquisition is described. The technique is called simultaneous multislice acquisition. Images generated using this technique are shown. Simultaneous multislice imaging is similar to a technique developed for line scanning by Mansfield *et al.* (*4, 5*). Instead of acquiring one line of the image at a time, the readout direction was tilted to allow several lines of the image to be acquired simultaneously.

In conventional imaging techniques, one set of echoes contains the image information for a single slice. When the simultaneous multislice technique is used, a set of echoes contains the image information for multiple slices. This new technique excites several parallel slices with each RF pulse. During the readout of an echo, two gradients are applied simultaneously: the usual readout gradient and the slice selection gradient. The readout gradient spreads the signal from each slice over the slice bandwidth. The slice bandwidth occupies a portion of the bandwidth sampled by the imager. The slice selection gradient adds a frequency offset to the signal from each slice. When the frequency offset is greater than the slice bandwidth, the bandwidths of the slices will not overlap; therefore, the slices appear side by side in the image after reconstruction.

The number of slices that can be obtained with the simultaneous multislice technique is limited only by the bandwidth of the imager, the accuracy of the RF pulse shape, and the maximum RF power. The spatial resolution in the readout direction deteriorates if the slices are located too close together. The voxels become more tilted and the images appear more blurred as the slices are brought closer together.

0740-3194/88 $3.00

I. IMPLEMENTATION

Most sequences can be modified to implement the simultaneous multislice technique. Implementation of the simultaneous multislice technique requires three modifications to a sequence: the RF pulses must excite multiple slices simultaneously, the slice selection gradient must be on during signal acquisition, and a larger bandwidth must be sampled.

(a) RF Pulses

RF pulses that excite several slices simultaneously can be produced. The normal slice selection pulse is a $\sin(t)/t$ function, where t is time. The position of the excited slice can be moved by multiplying the $\sin(t)/t$ function by a complex exponential in the time domain. A pulse that excites two parallel slices simultaneously is formed by adding two $\sin(t)/t$ functions that are multiplied by different complex exponentials. A convenient way to do this is to multiply the $\sin(t)/t$ function by a $\cos(dt)$. Because the $\cos(dt)$ is a sum of complex exponentials, this has the effect of exciting two slices which are located a distance, $d/2$, on either side of the original slice position. The $\sin(t)/t$ function multiplied by $\cos(dt)\cdot\cos(2dt)$ excites four slices. The four slices are also spaced a distance d apart. With this technique, the number of slices can be increased to any power of two, and all of the slices will be evenly spaced.

(b) Gradients and Bandwidth Utilization

A larger bandwidth can be sampled by decreasing the dwell time of the analog to digital converter; i.e., increasing the sampling rate increases the bandwidth sampled. In the simultaneous multislice technique, the bandwidth sampled, Δf, must be many times the bandwidth occupied by each slice, Δf_{slice}. The amount of the imager bandwidth that each slice occupies is determined by the size of the gradients turned on during signal acquisition.

The minimum separation between slices and the amount of blurring in the image are determined by the relative sizes of the readout and the selection gradients that are on during the echo acquisition. The bandwidth that each slice occupies, Δf_{slice}, is proportional to the strength of the readout gradient, G_{R}, and the field of view, F,

$$\Delta f_{\text{slice}} = \gamma \cdot G_{\text{R}} \cdot F, \qquad [1]$$

where γ is the gyromagnetic constant. The frequency offset between the slices, Δf_{offset}, is proportional to the strength of the selection gradient on during the echo, G_{S}, and the distance between the slices, d,

$$\Delta f_{\text{offset}} = \gamma \cdot G_{\text{S}} \cdot d. \qquad [2]$$

The slices will be separated completely in the reconstructed image only if the frequency offset, Δf_{offset}, is equal to or larger than the slice bandwidth, Δf_{slice},

$$\Delta f_{\text{offset}} \geq \Delta f_{\text{slice}} \qquad [3]$$

or

$$G_{\text{S}} \cdot d \geq G_{\text{R}} \cdot F. \qquad [4]$$

This relationship sets appro
minimum distance between
[4] will follow. The distance
ratio G_S/G_R. However, ther
increases as the ratio G_S/G_R
Δf_{depth}, along the voxel depth
gradient on during the acqui
portional to G_S and the slice

When Δf_{depth} is larger than
pixels are skewed; the pixel sl
blurred in the image. The t
bottom appears n_b voxels to t

where P is the dimension of
quantity n_b is an index of blu
slice with the effective readou
that as G_S/G_R is increased i
blurring increases. If n_b is ke
used a slice selection gradien
chemical-shift effects [6]. A
negligible in normal imaging

The precise relationship f
the slices in the image must i
image should be extended b
overlap the blurred edge of tl

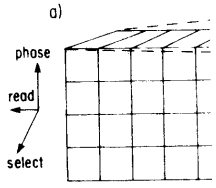

FIG. 1. (a) A group of voxels fro
volume. (c) The pixel skewing when
little blurring would result. The ne
perpendicular to the net gradient. (
($n_b = 3$). The blurring would be sign

This relationship sets approximate limits on the sizes of the gradients and on the minimum distance between the excited slices; a relation that is more realistic than [4] will follow. The distance between the slices can be minimized by maximizing the ratio G_S/G_R. However, there is a skewing or tilting of the voxels in the slice which increases as the ratio G_S/G_R increases. The skewing is caused by the frequency shift, Δf_{depth}, along the voxel depth. This skewing is caused by the presence of the selection gradient on during the acquisition. The frequency shift along the voxel depth is proportional to G_S and the slice thickness, T,

$$\Delta f_{depth} = \gamma \cdot G_S \cdot T. \qquad [5]$$

When Δf_{depth} is larger than the frequency shift across the voxel width, Δf_{width}, the pixels are skewed; the pixel skewing causes cylindrically symmetric objects to appear blurred in the image. The top of the voxel appears n_b voxels to one side and the bottom appears n_b voxels to the other side,

$$n_b = (G_S \cdot T/2)/(G_R \cdot P), \qquad [6]$$

where P is the dimension of the voxel in the direction of the readout gradient. The quantity n_b is an index of blurring in the image. Figure 1 shows a cross section of the slice with the effective readout gradient and the resulting voxel outlines. It can be seen that as G_S/G_R is increased in order to decrease the distance between the slices, the blurring increases. If n_b is kept small, negligible image blurring will result. Cho *et al.* used a slice selection gradient during data acquisition to eliminate susceptibility and chemical-shift effects [6]. A G_S/G_R of one was used; the blurring was reported to be negligible in normal imaging.

The precise relationship for the minimum frequency offset necessary to separate the slices in the image must include extra bandwidth for the blurring. The edge of the image should be extended by n_b pixels so that the blurred edge of one slice will not overlap the blurred edge of the next slice. The effective field of view has two edges, so

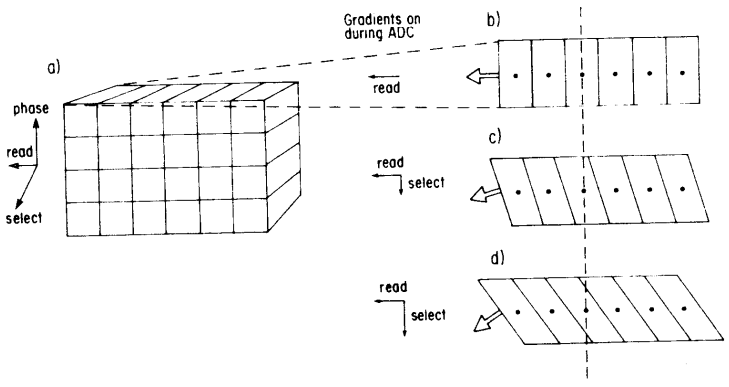

FIG. 1. (a) A group of voxels from a conventional imaging sequence. (b) A row of pixels from the volume. (c) The pixel skewing when a small selection gradient is on during data acquisition ($n_b = 1$); very little blurring would result. The net read gradient on during the ADC is shown; the pixel borders are perpendicular to the net gradient. (d) The effect of a large selection gradient on during data acquisition ($n_b = 3$). The blurring would be significantly larger.

it must be extended by $2n_b$ pixels. In practice, it is useful to have three or four pixels with no signal between the images. The effective field of view would be extended by $2n_b + 4$ pixels. The bandwidth each slice occupies is then

$$\Delta f_{slice} = \gamma \cdot G_R \cdot (F + (2n_b + 4) \cdot P). \quad [7]$$

By combination of [2], [3], [6], and [7], a more practical relationship among the gradient sizes, the field of view, and the minimum distances between the slices is obtained:

$$d_{min} = (G_R/G_S) \cdot (F + 4P) + T. \quad [8]$$

Equations [6] and [8] show the limitations of the simultaneous multislice technique as it is implemented on a conventional scanner. These limitations can be mitigated by limiting the field of view in the readout direction or by employing nonlinear pulsed gradients. Several techniques for limiting the field of view are being developed for spectroscopy; presaturation and surface coil techniques are the most common (*7–9*).

II. METHODS

(a) Sequences

The two sequences used to obtain multiple slices simultaneously are shown in Fig. 2. The sequences were implemented on a Siemens 1-T Magnetom. The first sequence is used to explore the limits of the technique: slice profiles, slice positions, number of slices obtainable, and pixel skewing. The second sequence is a FLASH sequence modified to implement the technique. The modified FLASH sequence is an example

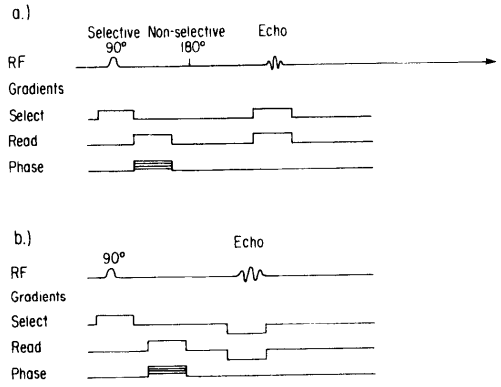

FIG. 2. The pulse sequence in (a) represents the sequence used to test the effects and extent of blurring for several gradient sizes and slice thicknesses. Two, four, eight, and sixteen simultaneous slices were obtained with this sequence. The 180° pulse was nonselective. Therefore, standard multislice acquisitions are not possible with this sequence. The pulse sequence in (b) represents a FLASH sequence modified to obtain simultaneous multiple slices. This sequence is used as an example; most standard sequences can be modified to obtain simultaneous multiple slices. The FLASH sequence can operate with both simultaneous multiple slice acquisition and standard multislice acquisition.

of a clinical sequence implementin
standard sequences can be modifi
technique.

The RF pulse shapes were $\sin(t)$
shapes were generated by a FORTRA
mize ghost images of excited spins b
functions on an infinite domain.

Both sequences in Fig. 2 sampled
resulting sampling times were longe
sampling times resulted in longer ech
mum bandwidth of the imager, 25
from the raw data with a FORTRAN

The slice separation was measure
ing and readout gradients were turn
as that in the imaging sequence. The
images showed the slice profiles alc
quence used nonselective RF pulse
phantom. The length of the phantc
slices measured with the first sequen

(b) Image Blurring vs Slice Separat

The sequence shown in Fig. 2a wa
size of the readout gradient was kept
gradient was changed to vary the a
effect of increased slice thickness wa
for each gradient strength was found
pulse calculation until the resulting
ground intensity between them. Th
then used to measure the slice separa

(c) Volume Imaging

The modified FLASH sequence sl
can be imaged in a short period of t
of performing both conventional mu
For example, if a conventional FLA
per slice, 6 slices can be imaged. Th
slice simultaneous multislice imagin
TR; i.e., 16 slices are imaged simulta
FLASH sequence.

A 190-mm-long, 90-mm-diamete
mm-thick slices in 47 s. The FLASH
ms. Six images were obtained; each i
sections of the phantom. The minim
was used.

of a clinical sequence implementing the simultaneous multislice technique; most standard sequences can be modified to implement the simultaneous multislice technique.

The RF pulse shapes were $\sin(t)/t$ functions as described previously. The pulse shapes were generated by a FORTRAN program. A Hamming filter was used to minimize ghost images of excited spins between the slices produced by finite sampling of functions on an infinite domain.

Both sequences in Fig. 2 sampled the echo with 1024 data points 15 μs apart. The resulting sampling times were longer than those of standard sequences; the longer sampling times resulted in longer echo times than those usually employed. The maximum bandwidth of the imager, 25 kHz, was used. The images were reconstructed from the raw data with a FORTRAN program.

The slice separation was measured with two sequences in which the phase-encoding and readout gradients were turned off. The selection gradient was kept the same as that in the imaging sequence. The first sequence used selective pulses. The resulting images showed the slice profiles along the length of the phantom. The second sequence used nonselective RF pulses. The resulting images showed a profile of the phantom. The length of the phantom was used to calibrate the distances between slices measured with the first sequence.

(b) Image Blurring vs Slice Separation and Slice Thickness

The sequence shown in Fig. 2a was used to image a 19-cm-diameter phantom. The size of the readout gradient was kept constant at 0.65 mT/m. The size of the selection gradient was changed to vary the amount of blurring observed in the images. The effect of increased slice thickness was also observed. The minimum slice separation for each gradient strength was found by increasing the separation factor, d, in the RF pulse calculation until the resulting images had a perceptible distance of flat, background intensity between them. The sequences without the readout gradient were then used to measure the slice separation.

(c) Volume Imaging

The modified FLASH sequence shown in Fig. 2b was used to show that a volume can be imaged in a short period of time. The modified FLASH sequence is capable of performing both conventional multislice and simultaneous multislice acquisitions. For example, if a conventional FLASH sequence with a TR of 0.32 s requires 50 ms per slice, 6 slices can be imaged. The FLASH sequence modified to implement 16-slice simultaneous multislice imaging can generate images of 96 slices with the same TR; i.e., 16 slices are imaged simultaneously for each slice imaged in the conventional FLASH sequence.

A 190-mm-long, 90-mm-diameter phantom was imaged with 94 consecutive 2-mm-thick slices in 47 s. The FLASH images are T2 weighted; TR = 0.32 s, TE = 25 ms. Six images were obtained; each image has sixteen 2-mm simultaneous multislice sections of the phantom. The minimum slice spacing or the maximum ratio G_S/G_R was used.

III. RESULTS AND DISCUSSION

(a) The sequences shown in Fig. 2 were implemented on a Siemens 1-T Magnetom. The sequences produced images of phantoms with no major problems. All images were obtained with the head coil of the Magnetom. An example of a simultaneous eight-slice acquisition is shown in Fig. 3.

Adjusting the RF transmitter and receiver gains was done manually because the automatic adjustment routines did not operate for the RF pulses used here. Manual adjustment is difficult, time consuming, and not very accurate. Image quality could be improved significantly by improving the receiver gain calculation. Minimizing the excitation of spins between the slices by optimizing the RF envelope would also be productive.

(b) The trade-off between minimum slice separation and image blurring is illustrated in Fig. 4. The resolution portion of the 19-cm-diameter phantom is shown for a conventional image and for three values of the blurring index, n_b. The values of n_b, the minimum slice separation, and the ratio of the gradient strengths G_S/G_R for the four images are shown in Table 1. The blurring in Fig. 4b is just discernible. The blurring in Fig. 4c is distinct. The blurring in Fig. 4d renders the image of limited usefulness.

The blurring caused by increasing the slice thickness is demonstrated in Fig. 4e. The slice shown in Fig. 4e has the same G_S/G_R as that of Fig. 4c but is twice as thick, i.e., 4 mm thick. Therefore, the slices shown in Figs. 4d and 4e have the same value of n_b. The blurring is the same.

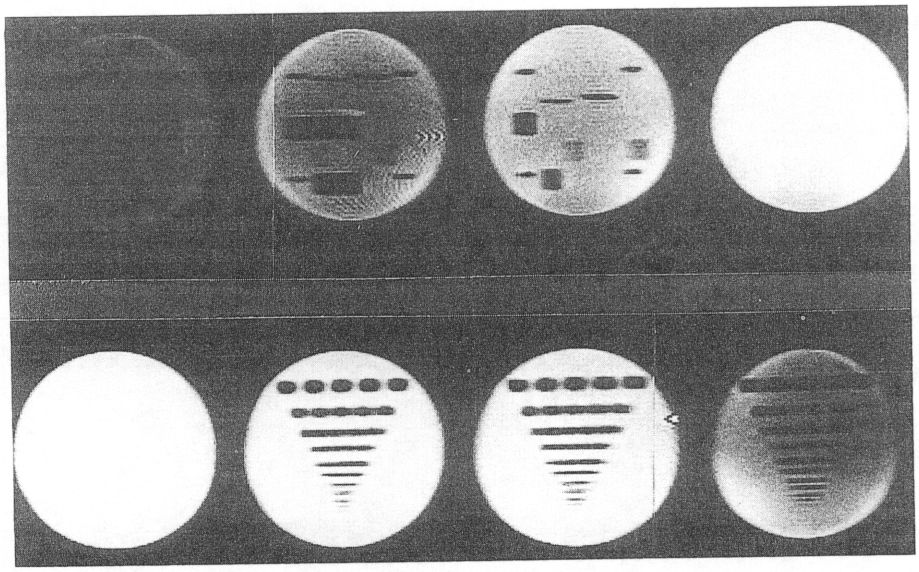

FIG. 3. An eight-slice simultaneous multislice acquisition. The slices are 2 mm thick and 2.4 cm apart. The drop off of intensity away from the center of the image is due to the 25-kHz lowpass filter of the system.

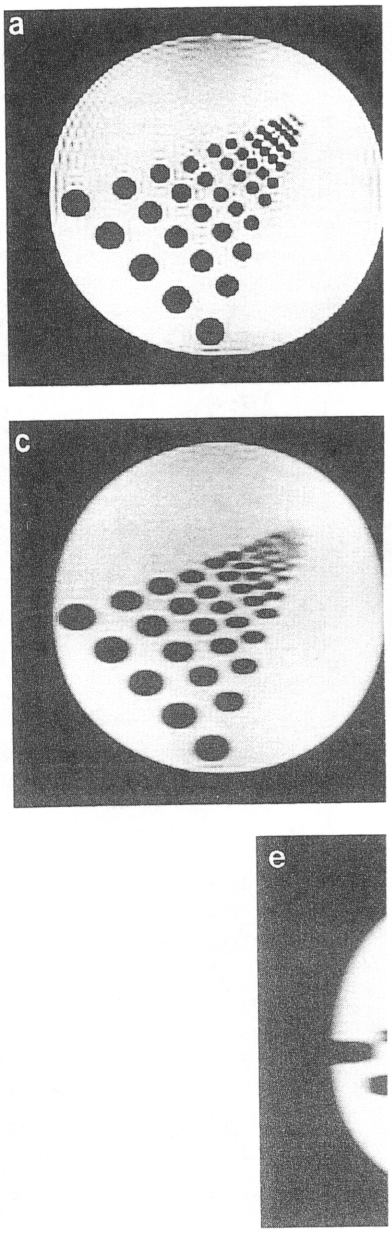

FIG. 4. The image blurring caused by s
shown in (a). The sequence in Fig. 2a was
(c), and 9.2 (d). Images (a, b, c, and d) are
A 4-mm-thick slice with G_S/G_R of 4.6; the
the values of n_b for the slices shown.

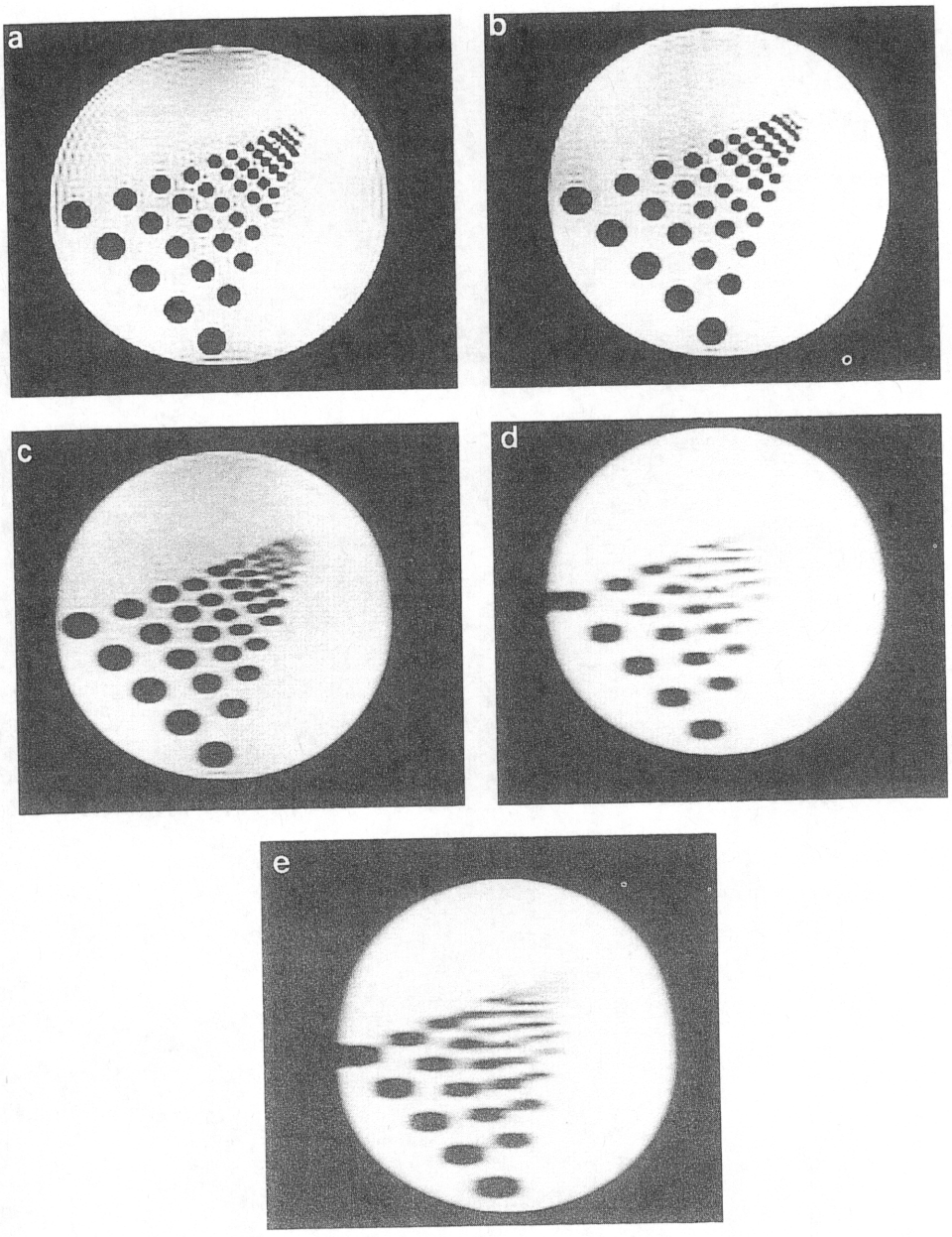

FIG. 4. The image blurring caused by simultaneous multislice acquisition. A conventional image is shown in (a). The sequence in Fig. 2a was used to obtain three images with G_S/G_R values of 1.5 (b), 4.6 (c), and 9.2 (d). Images (a, b, c, and d) are 2 mm thick, TR = 0.4 s, TE = 38 ms, and 2 mm pixel size. (e) A 4-mm-thick slice with G_S/G_R of 4.6; the value of n_b in this slice is the same as that in (d). Table 1 shows the values of n_b for the slices shown.

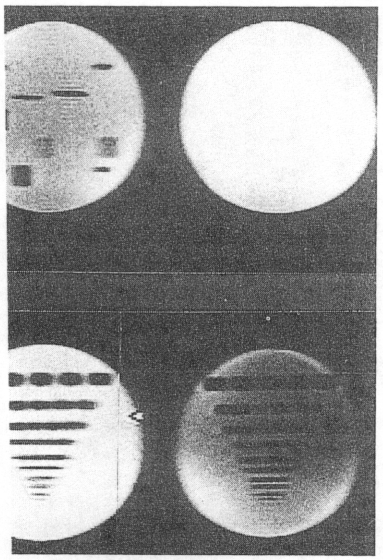

he slices are 2 mm thick and 2.4 cm apart.
ıe to the 25-kHz lowpass filter of the system.

TABLE 1

Minimum Slice Separation Measured and Calculated with Eq. [8] for the Three Gradient Ratios Used to Produce the Images in Fig. 4

Ratio G_S/G_R	Blurring index n_b	d minimum (mm)			
		190-mm field of view		90-mm field of view	
		Calculated	Measured	Calculated	Measured
9.2	7.9	24	24	13	13
4.6	3.9	45	45	24	24
1.5	1.3	135	135	68	71

Note. Pixel size, P, is 2.3 mm and slice thickness, T, is 2 mm.

Figure 5 shows a comparison between a pair of slices imaged simultaneously and images obtained with a conventional spin-echo sequence. The images in Fig. 5a were obtained with the simultaneous multislice technique; the value of n_b is 1.3. The images in Figs. 5b and 5c were obtained with a conventional spin-echo sequence. The

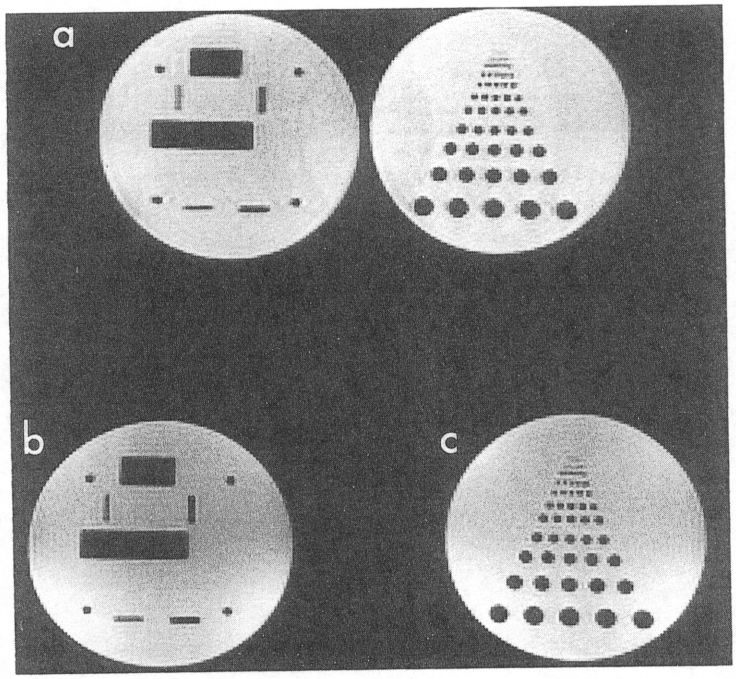

FIG. 5. Images obtained from three acquisitions using identical parameters; TR = 0.25, TE = 38 ms, slice thickness = 2 mm, and 128 matrix. (a) Obtained with the simultaneous multislice technique; the blurring index, n_b, is 1.3. (b and c) Generated with two conventional acquisitions of the same two slices. Minimal image degradation is observed in the readout direction of the simultaneous multislice images.

same parameters were used in al
dation in the simultaneous mult

(c) Figure 6 shows one of the
fied to implement simultaneous
the homogeneous phantom in th
is caused by the roll-off of the lo
end slices show significant degr
slices obtained from each of the
was imaged with 2-mm slices in
measurement times on the orde
we currently use requires a TR
phantom could be imaged with
min. The increase in the numbe
multislice technique is dramatic
sition of large numbers of slices

A method that produces simu
has been presented. For slice se
the readout direction there is ve

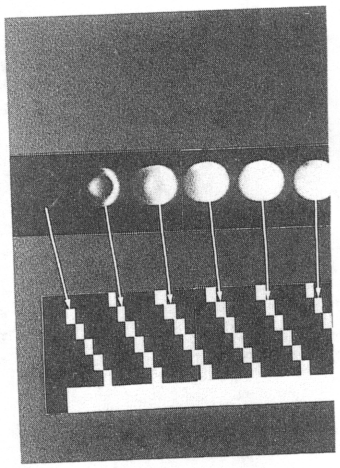

FIG. 6. Shows one of the six images
simultaneous multislice and conventic
mm-diameter sections side by side. Tl
shows the position of each section in th
with no phase or readout gradients; the
The sequences used are described unde
it is 190 mm long. The other six row
multislice capability of the sequence.
indicate the position of each section in
axial sections in 47 s.

\VER

with Eq. [8] for the Three Gradient Ratios
ages in Fig. 4

d minimum (mm)		
w	90-mm field of view	
asured	Calculated	Measured
24	13	13
45	24	24
35	68	71

ım.

of slices imaged simultaneously and
sequence. The images in Fig. 5a were
nique; the value of n_b is 1.3. The im-
nventional spin-echo sequence. The

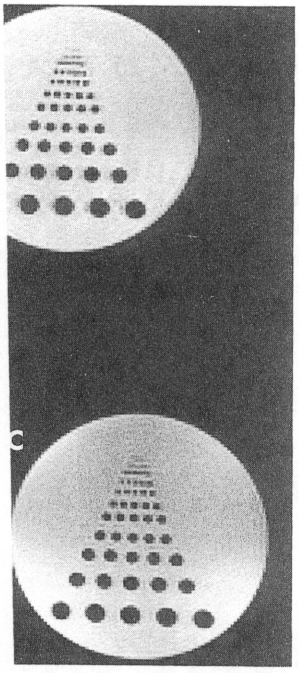

ıtical parameters; TR = 0.25, TE = 38 ms,
the simultaneous multislice technique; the
entional acquisitions of the same two slices.
ın of the simultaneous multislice images.

same parameters were used in all three acquisitions. There is very little image degradation in the simultaneous multislice images.

(c) Figure 6 shows one of the 6 images obtained from the FLASH sequence modified to implement simultaneous multislice capabilities. This image has 16 sections of the homogeneous phantom in the same image. The darkness of the ends of the image is caused by the roll-off of the low pass filter. A wider low pass filter is needed. The end slices show significant degradation. Figure 6 also shows the position of the 16 slices obtained from each of the 6 images of the phantom. The entire 190 mm length was imaged with 2-mm slices in 47 s. Three-dimensional FLASH sequences require measurement times on the order of 10 min (*3*). The conventional FLASH sequence we currently use requires a TR of 32.2 ms per slice. Therefore, the 190 by 90-mm phantom could be imaged with 2-mm axial slices in $6\frac{1}{2}$ min or with sagittal slices in 3 min. The increase in the number of slices that can be obtained with the simultaneous multislice technique is dramatic. However, the image quality for simultaneous acquisition of large numbers of slices must be improved significantly.

IV. CONCLUSIONS

A method that produces simultaneously acquired images of multiple parallel slices has been presented. For slice separations approximately equal to the field of view in the readout direction there is very little image degradation. Slice separations as small

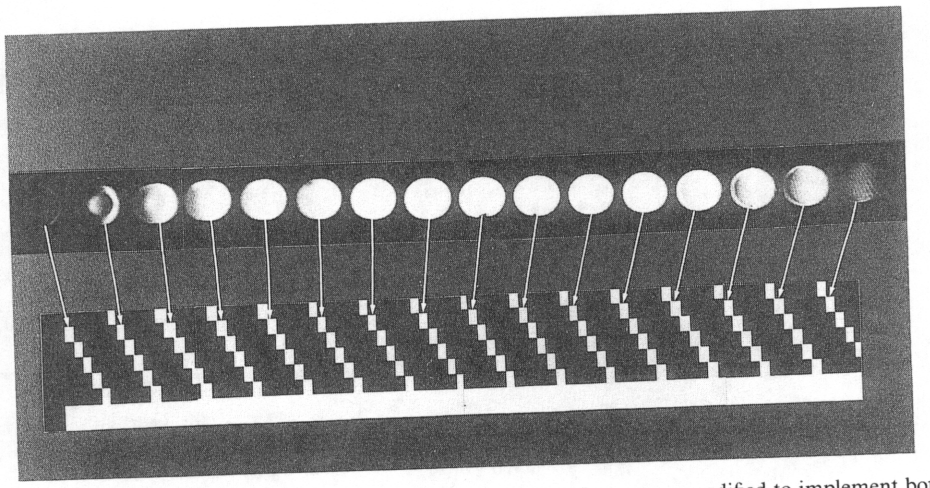

FIG. 6. Shows one of the six images obtained with the FLASH sequence modified to implement both simultaneous multislice and conventional multislice capabilities. Each of the six images shows sixteen 90-mm-diameter sections side by side. The parallel sections are 12 mm apart. The bottom of the figure also shows the position of each section in the phantom. These are views of the phantom and the excited sections with no phase or readout gradients; therefore, these are side views of the phantom and the sections imaged. The sequences used are described under Methods. The solid bar is a side view of the extent of the phantom; it is 190 mm long. The other six rows are side views of the six images obtained with the conventional multislice capability of the sequence. The white lines is each row are side views of the sections imaged and indicate the position of each section imaged. The entire phantom was imaged with ninety-four 2-mm-thick axial sections in 47 s.

as 15% of the field of view can be used, but significant image blurring occurs. Techniques to limit the field of view in the readout direction should be developed to allow closely spaced slices. The simultaneous multislice technique can be used productively in at least two situations: to extend the number of slices obtained without increasing the repetition time and to image volumes in very short times.

ACKNOWLEDGMENTS

I am grateful to Michael Silver, of Siemens Medical Systems, for his information and ideas on RF pulse programming. I acknowledge the helpful support of and discussions with Peter K. Spiegel.

REFERENCES

1. A. HAASE, J. FRAHM, D. MATTHAEI, W. HANICKE, AND R. D. MERBOLDT, *J. Magn. Reson.* **67,** 258 (1986).
2. J. FRAHM, A. HAASE, AND D. MATTHAEI, *Magn. Reson. Med.* **3,** 321 (1986).
3. D. MATTHAEI, J. FRAHM, A. HAASE, W. HANICKE, AND K. D. MERBOLDT, *Magn. Reson. Imaging* **4,** 381 (1986).
4. P. MANSFIELD AND A. A. MAUDSLEY, *J. Magn. Reson.* **27,** 101 (1977).
5. P. MANSFIELD AND I. L. PYKETT, *J. Magn. Reson.* **29,** 355 (1979).
6. Z. H. CHO, D. J. KIM, AND Y. K. KIM, *Med. Phys.* **15**(1), 7 (1988).
7. P. R. LUYTEN, A. J. H. MARIEN, B. SIJTSMA, AND J. A. DEN HOLLANDER, *J. Magn. Reson.* **67,** 148 (1986).
8. R. T. BOGUSKY, M. GARWOOD, G. B. MATSON, G. ACOSTA, L. D. COWGILL, AND T. SCHLEICH, *Magn. Reson. Med.* **3,** 251 (1986).
9. M. GARWOOD, T. SCHLEICH, AND M. R. BENDALL, *J. Magn. Reson.* **73,** 191 (1987).

MAGNETIC RESONANCE IN MEDICINE **8,** 285-

Gastrointestinal Contras

JAY J. LISTINSKY

Departments of Radiology† and E
Roch

Received Janua

The clay minerals kaolin and be
agents for MRI. Weak field depenc
of these agents at all field strengths
their immediate environment and a

I

Magnetic resonance (MR) imagi
assessment of lesions in the liver (
and many types of liver lesions is rea
sequences. Evaluation of abdomina
hampered by the lack of a reliable m
The distinction cannot always be
images is not always easily predict
anatomy. Loops of bowel may be
lesions, enlarged lymph nodes, or i
evaluate because the adjacent stom
pancreas or may simulate the appea
A need exists for a safe and effective
from other abdominal structures.

One solution to this problem is th
computed tomography of the body,
or by rectum to provide image contr
bowel contrast agent would be char
pulse sequences and magnetic field
toxicity, and low cost of the essenti
bowel contrast agents include paran
superparamagnetic particles (*4*), and
als is less than ideal in one or more re
specifically, clay minerals in aqueo
vitro and *in vivo*. The combination
of the raw materials makes these cla

‡ Present address: Department of Radiolo